ANNUAL REVIEWS

Annual Review of Nuclear and Particle Science

Astrophysical Sources of High-Energy Neutrinos in the IceCube Era

P. Mészáros

Department of Astronomy and Astrophysics, Department of Physics, Center for Particle and Gravitational Astrophysics, Pennsylvania State University, University Park, Pennsylvania 16802; email: nnp@psu.edu

Annu. Rev. Nucl. Part. Sci. 2017. 67:45–67

First published as a Review in Advance on July 31, 2017

The *Annual Review of Nuclear and Particle Science* is online at nucl.annualreviews.org

https://doi.org/10.1146/annurev-nucl-101916-123304

Copyright © 2017 by Annual Reviews.
All rights reserved

ANNUAL REVIEWS **Further**

Click here to view this article's online features:

- Download figures as PPT slides
- Navigate linked references
- Download citations
- Explore related articles
- Search keywords

Keywords

neutrino astrophysics, cosmic rays, cosmic backgrounds, galaxies, massive stars, black holes

Abstract

High-energy neutrino astrophysics has come of age with IceCube's discovery of neutrinos in the TeV to PeV energy range, attributable to extragalactic sources at cosmological distances. At such energies, astrophysical neutrinos must originate in cosmic-ray interactions, providing information about the sources of high-energy cosmic rays, as well as leading to the coproduction of high-energy γ-rays. The intimate link with these two independently observed types of radiation provides important tools for the quest to identify and understand the nature of the astrophysical sources of the neutrinos. These neutrinos can set important constraints on the cosmic-ray acceleration process, and because they travel essentially unimpeded, they can probe our Universe out to the farthest cosmological distances.

Contents

1. VERY HIGH ENERGY NEUTRINO OBSERVATIONS

The exciting discovery (1–3) of a diffuse flux of TeV to $\gtrsim$PeV neutrinos of definite astrophysical origin was achieved with the cubic-kilometer IceCube Cherenkov neutrino detector (4). This discovery was the culmination of a series of increasingly sophisticated experimental developments and observation campaigns; notable achievements in this search were attained through the DUMAND concept (5), the Baikal experiment (6), and the ANTARES experiment (7).

The flux of very high energy (VHE) neutrinos observed by IceCube includes both cascade events ascribed to ν_e, anti-ν_e, ν_τ, and anti-ν_τ; angular resolutions of $\sim$15–30°; and tracks ascribed to ν_μ and anti-ν_μ, with angular resolutions of $\sim$1°. The spectrum clearly departs from that of the atmospheric neutrino background with $\geq 7\sigma$ significance (**Figure 1*a***).

The flavor ratio is compatible with a (ν_e+anti-ν_e):(ν_μ+anti-ν_μ):(ν_τ+anti-ν_τ) distribution, as expected from pion decay followed by vacuum oscillations across cosmological distances (**Figure 1*b***) (10). Regarding the directions from which the individual neutrinos arrive at Earth, there is no hint of a concentration toward either the Galactic Center or the plane, the directions being compatible with an isotropic flux (11); nor is there any significant correlation with the arrival direction of ultrahigh-energy cosmic rays (UHECRs) detected by Pierre Auger (Auger) or the Telescope Array (TA) (12). Although there is no significant correlation with any class of extragalactic objects, the isotropicity of the neutrino flux strongly suggests that it is of extragalactic origin.

2. GENERIC SOURCE REQUIREMENTS

A precondition for likely astrophysical VHE neutrino sources is that they be sources of VHECRs, or that they be irradiated by a flux of CRs from some other source(s). So far, the isotropicity of the IceCube events has led to the search for possible candidates concentrated mainly in extragalactic space (e.g., 13). Such sources could also be naturally related to the sources of UHECRs observed by the Auger and TA CR arrays (12), although for the currently detected maximum neutrino energies of $\lesssim$3 PeV it is only necessary to have sources capable of accelerating CRs up to $\lesssim$100 PeV, as discussed below.

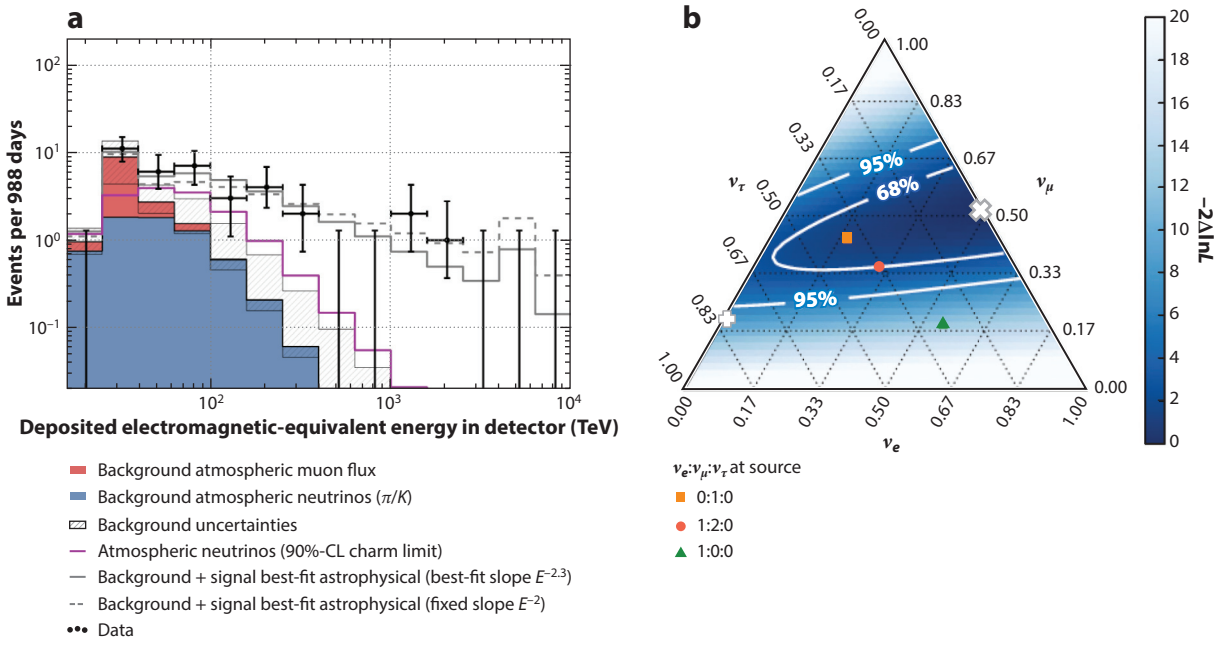

Figure 1

(*a*) All-flavor spectrum of very high energy neutrinos detected by IceCube (modified from Reference 8; also see Reference 9). (*b*) Flavor ratio probability distribution of astrophysical neutrinos above 35 TeV detected by IceCube (9).

The spectrum shown in **Figure 1** can in principle be produced by a CR spectrum of roughly $N(E_p) \sim E_p^{-2.5}$, which is steeper than the −2 to −2.2 slope expected from first-order Fermi acceleration. The latter spectrum, if extending above ∼100 PeV for CRs, would have resulted in a peak around 6.3 PeV in the anti-ν_e component due to the Glashow resonance (e.g., 14–20). So far, this resonance has not been observed; IceCube has detected only upper limits above ∼3.5 PeV. Either the diffuse spectrum is a single power law of slope ∼−2.5, or, if the spectrum is flatter below ∼6.3 PeV, there could be a spectral break above a few PeV, which could arise naturally in some systems due to a steepening of the CR diffusion coefficient (e.g., 14, 21–23).

The *Fermi* diffuse isotropic γ-ray background in the ∼10–800-GeV photon energy range imposes serious constraints on essentially all pp neutrino sources, and on most $p\gamma$ sources as well, because of the comparable fraction of π^0 production resulting in secondary TeV to PeV γ-rays that cascade against the infrared and microwave extragalactic background light (EBL) and end up in the *Fermi* range (**Figure 2**). At birth, secondary γ-rays have the same slope as that of neutrinos, and the branching ratio of charged to neutral pions in pp (or $p\gamma$) interactions implies that the two flux levels are related through $E_\gamma^2 \Phi_{E_\gamma} = 2E_\nu^2 \Phi_{E_\nu}$. These initial γ-rays of energy $E_\gamma \gtrsim m_e^2/E_{\rm EBL}$ pair-produce against very low energy infrared photons of the diffuse EBL from stars, as well as the cosmic microwave background. The pairs then inverse-Compton-scatter against the same background of infrared photons, resulting in new, lower-energy γ-rays, and so forth. The resulting electromagnetic (EM) cascades lead to a universal spectral shape (26) that converts all the high-energy γ-rays into low-energy, sub-TeV photons. *Fermi*'s sensitivity in the ∼0.1–800-GeV range (27) provides strong constraints on models, in particular on the hadronuclear origin of neutrinos from any type of source (**Figure 2**) (e.g., 14, 22–25, 28–31).

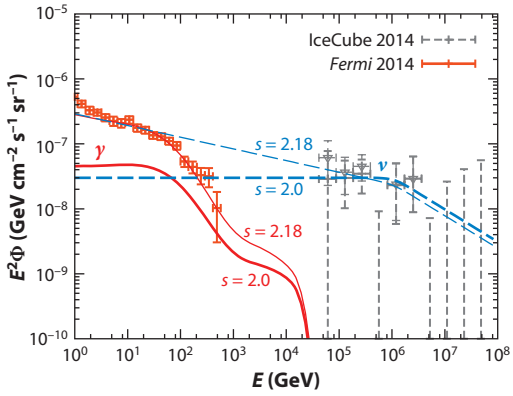

Figure 2

The isotropic γ-ray background observed by *Fermi* compared with the diffuse per flavor neutrino flux observed by IceCube. The gray lines represent possible neutrino models consistent with IceCube data; the red lines represent the corresponding γ-rays of pp scenarios reprocessed in the external background light (EBL). The thick and thin solid lines show a power law with slope $s = 2.18$ and $s = 2.0$, respectively, with an exponential cutoff around PeV. Modified from Reference 24; also see Reference 25.

A dominant fraction of the *Fermi* diffuse extragalactic γ-ray background is accounted for by unresolved distant blazars (27), whose γ-ray emission is most likely of leptonic origin (i.e., due to mechanisms that are not associated with neutrinos). By contrast, many of the most commonly considered sources, such as active galactic nuclei (AGNs), standard γ-ray bursts (GRBs), and so forth, would be optically thin; that is, they would allow the free escape of both neutrinos and γ-rays, the latter being restricted by *Fermi* observations. This restriction would not apply, however, to so-called EM-hidden sources (e.g., 32), in which $p\gamma$ or pp γ-rays are either absorbed or degraded to substantially lower energies, making such sources less (or not at all) constrained by *Fermi*.

For sources dominated by pp, the efficiency (or optical depth) $\tau_{\gamma\gamma}$ of $\gamma\gamma$ absorption is generally uncorrelated to its pp pion formation efficiency f_{pp}, given that the former depends on the photon target column density and the latter on the proton target column density. For $p\gamma$ sources, however, there is a generic correlation (33) between $\tau_{\gamma\gamma}$ and $f_{p\gamma}$, as both depend on the photon target column density. The $p\gamma$ opacity is $\kappa_p \sigma_{p\gamma} \sim 0.7 \times 10^{-28}$ cm^2, where κ_p is the inelasticity, whereas the $\gamma\gamma$ opacity is $\sigma_{\gamma\gamma} \sim 0.1\sigma_{\rm T}$, where $\sigma_{\rm T}$ is the Thomson cross section; therefore, $\tau_{\gamma\gamma} \sim \sigma_{\gamma\gamma}/(\kappa_p \sigma_{p\gamma}) f_{p\gamma} \sim 10^3 f_{p\gamma}$ (e.g., 32). Thus, for moderately efficient $p\gamma$ sources, high-energy γ-rays will be efficiently degraded. The final energy at which they reappear after the cascades depends on the target photon energy spectrum. In addition, because the $\gamma\gamma$ cross section is close to that of Compton scattering, the photons can be trapped and partially thermalize as they diffuse out. This is important for sources such as AGNs, standard GRBs, or others that have also been detected in the optical, X-ray, or MeV range, where additional constraints are imposed by stacking analyses of source locations against the error boxes of individual detected neutrinos. Thus, in general, compact high-energy sources such as GRBs, especially choked GRBs (34, 35), white dwarf mergers (36), tidal disruption events (37, 38), core AGN sources (39), and so forth, by virtue of their high photon density are likelier to suffer photon trapping and efficient $\gamma\gamma$ degradation, making them EM dim or effectively EM hidden. As discussed in Section 3.1, another way in which neutrino and γ-ray sources can be electromagnetically hidden in the *Fermi* range is if they are at high redshifts, $z \gtrsim 3$–4 (40, 41); the longer path length ensures more efficient absorption in the EBL.

3. SPECIFIC ASTROPHYSICAL SOURCES

3.1. Active Galactic Nuclei

The term AGN is applied to a small fraction of all galaxies in which either the galactic nucleus is a prominent source of radio, optical, or X-ray photons or else (or in addition) it has bright jets emanating from the nucleus, which are detectable in the radio, optical, X-ray, or γ-ray range. These emissions are powered by accretion onto a central massive black hole (MBH) in the nucleus. An average galaxy such as the Milky Way generally also has an MBH at its center, and in ~30% of such galaxies, the gas accreting into the MBH leads to detectable radio or X-ray emission in the range of 10^{43} erg s^{-1}. These galaxies are called low-luminosity AGNs (LLAGNs). AGNs can have luminosities up to four to five orders of magnitude higher than that of LLAGNs, and they are subdivided into radio-quiet (RQ) AGNs (a misleading term, as they have a dominant radio or X-ray nuclear emission that is also present in LLAGNs) and radio-loud (RL) AGNs, which show luminous jets, detected mostly in radio but in some cases also in the optical, X-ray, and/or γ-ray range. RQ and RL AGNs represent roughly 10^{-1} and 10^{-2} of the total galaxy population, respectively. RL (jet) AGNs are further subdivided into the so-called FR-I and FR-II types. FR-I galaxies have irregularly shaped, low-luminosity outer jets extending not far beyond the host galaxy; the nearest ones sometimes show a bright, very straight inner jet inside the galaxy image.[1] FR-II galaxies have very extended, high-luminosity narrow jets whose dimensions (up to a few hundred kpc) can far exceed those of the optical host galaxy.

Blazars are a rare subclass of RL AGNs (~10^{-5} of all galaxies) whose jets point close to the line of sight. The jets are relativistic (bulk Lorentz factors $\Gamma_j \sim 5$–30), implying a large Doppler boost of the jet luminosity that dominates that of the host galaxy and the nucleus. Blazars include aligned FR-I AGNs, called BL Lac objects, whose luminosities are not overly high (~10^{44}–10^{45} erg s^{-1}), and aligned FR-II AGNs, called flat-spectrum radio quasars (FSRQs),[2] whose luminosities are much higher $\lesssim 10^{46}$–10^{47} erg s^{-1}) (**Figure 3**).

Models can generically be classified as leptonic, hadronic, or leptohadronic, depending on how important the EM emission of the hadronic secondaries is for the observed photon spectra. In leptonic models it is the primary accelerated electrons that are responsible for the photon spectra, even if the hadrons were accelerated (their secondary EM emission is negligible). In hadronic models the hadronic secondary EM emission (or, in some cases, proton synchrotron) provides the bulk of the observed EM spectra, whereas in leptohadronic models it is a mixture of both. Protons may be accelerated in all three types, and the CR efficiency is generally parameterized with the ratio of the luminosities in CRs and photons:[3] $\xi_{\rm CR} = L_{\rm CR}/L_{\rm rad}$.

RL AGNs, especially blazars, were the earliest suspected CR accelerator candidates. Their relativistic jets undergo strong shocks as they plow into the intergalactic medium (IGM), made detectable by the intense nonthermal radiation ascribed to synchrotron and inverse Compton radiation from relativistic electrons, which are presumed to be accelerated into a power law distribution by a Fermi process in high-Mach-number shocks. These termination shocks, as well as internal shocks closer in within the jet, are also ideal sites for accelerating protons, and could be the source of the observed UHECRs as well as high-energy γ-rays (e.g., 43, 44) and VHE neutrinos (e.g., 45, 46). The production of such secondary γ-rays and neutrinos requires that the

[1] Examples are the radio, optical, and X-ray jets of the famous nearby M87 galaxy.

[2] Quasars are AGNs powered by the most massive MBHs (10^8–$10^{10} M_\odot$); they are called QSOs when detected only in the optical range and QSRs when detected in the radio range.

[3] Some authors use a ratio of CR luminosity to jet kinetic luminosity: $\xi'_{\rm CR} = L_{\rm CR}/L_{\rm kin}$.

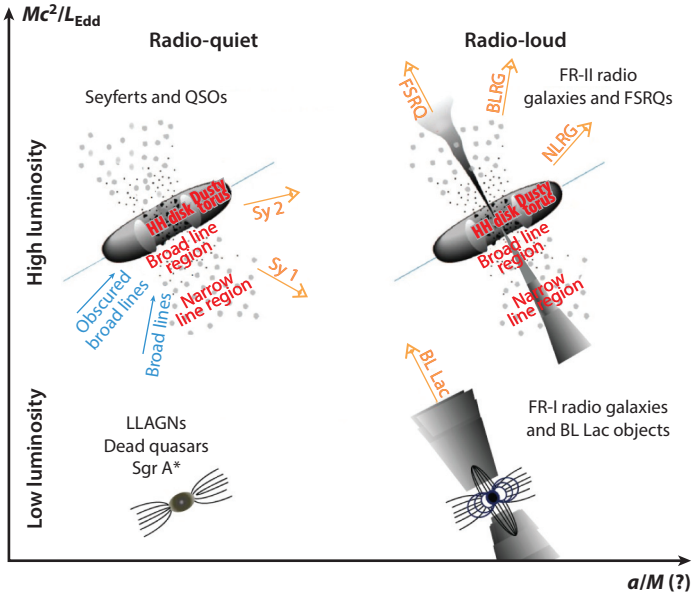

Figure 3

Types of active galactic nuclei (AGNs) with relative radio loudness on the *x* axis and luminosity on the *y* axis and an arbitrary division at 10^{45} erg s^{-1} between low-luminosity AGNs (LLAGNs) and high-luminosity AGNs (HLAGNs) (e.g., 42). Abbreviations: BLRG, broad line radio galaxy; FSRQ, flat-spectrum radio quasar; NLRG, narrow line radio galaxy; QSO, quasar detected in the optical range. Modified from Reference 42.

jet environment provide an adequate column density (or optical depth) of target photons and/or nucleons. Such targets are undoubtedly present, but the jets combine low target densities n_t, competing with their large dimensions R, to produce the optical depth $\tau_{pt} \sim n_t \sigma_{pt} R$ against proton or photon targets that make pions, leading to neutrinos and γ-rays (e.g., 47, 48).

In blazars, there are four main sources of photons that act as targets for $p\gamma$ interactions:

1. Continuum photons from the optically thick accretion disk that feeds the MBH, typically ranging over ~10–10^5 eV.
2. Continuum infrared photons from a dusty torus, which is often detected outside the accretion disk, typically peaking around ~10^{-2}–10^{-1} eV.
3. Line (H$\alpha \sim 10$ eV) photons from the so-called broad line region (BLR) gas clouds detected outside the jet, especially in FSRQs; the BLR also scatters disk and torus continuum photons toward the jet.
4. Nonthermal emission from the inner jet. In the so-called high-synchrotron-peaked (HBL) BL Lac objects, which can be detected up to TeV photon energies, this emission is a two-humped spectrum attributed to synchrotron and synchrotron self-Compton (SSC) radiation, whereas in the low-synchrotron-peaked (LBL) BL Lac objects and FSRQs, the two humps are best fitted with jet synchrotron radiation accounting for the low-energy peak and external Compton radiation accounting for the higher peak (i.e., scattering by jet electrons of "external" photons coming from the accretion disk; the dust torus; or, in FSRQs, the BLR's own Hα line photons plus the continuum disk and torus photons that it scatters into the jet).

In addition to blazars, other types of AGNs may contribute to the neutrino background. These include RQ quasars (e.g., 45, 49, 50) and LLAGNs (39). The CR acceleration and neutrino

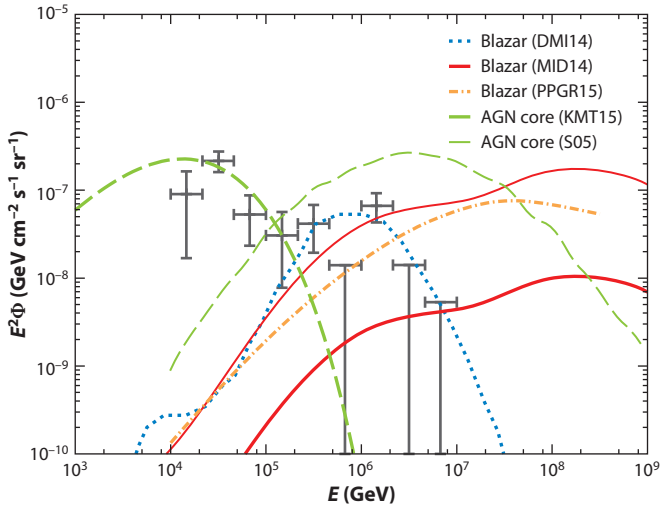

Figure 4

All-flavor diffuse neutrino intensity for various active galactic nuclei (AGN) jet and core models (51): DMI14, a flat-spectrum radio quasar jet model normalized to the IceCube data at PeV energies assuming $\langle z \rangle = 2$ (52); MID14, two different leptonic blazar jet models with high/low cosmic-ray efficiencies (47); PPGR15, a BL Lac jet model based on a leptohadronic scenario (53); KMT15, a low-luminosity AGN core model (39); and S05, a radio-quiet AGN core model (54). The diffuse neutrino intensity data are from the IceCube combined likelihood analysis (9).

emission of such RQ and LLAGN models are concentrated in the nucleus, where densities are higher. Because $\sigma_{pp} \sim 3 \times 10^{-26}$ cm^2 while $\sigma_{p\gamma} \sim 10^{28}$ cm^{-2} near threshold, although the relative increase of the nucleon density is greater than that of the photons, the pp interactions can become more important or even dominant.

Figure 4 (51) compares the diffuse neutrino background predictions from some of the AGN models with IceCube data (9). Typical blazar models have hard spectra because the $p\gamma$ efficiency increases linearly with energy, and for a proton slope of -2 or -2.5 the neutrino spectrum has a positive slope. These models can explain the PeV data, but they underpredict the TeV data. Also, these models are in tension with the nonobservation of a Glashow resonance at 6.3 GeV. The exception is an FSRQ model (52) in which protons are accelerated by a Fermi second-order mechanism and the maximum proton energy at which acceleration balances escape is ~10–100 PeV, whereas the main targets are BLR photons of ~10 eV, which yields a neutrino cutoff in the few-PeV range. Older AGN core models have similar problems with the Glashow resonance and also underpredict the TeV data. A more recent LLAGN core model (39), assuming a radiatively inefficient accretion flow (RIAF) in which pp interactions dominate, reproduces well the 10–100-TeV data but underpredicts the PeV data. These are typically one-zone models, which involve large astrophysical uncertainties; therefore, although they all appear to encounter difficulties in fitting the spectral data, they may not necessarily be ruled out. Other, weaker AGNs that have been considered are radio galaxies (e.g., 55, 56).

An important observational constraint has been provided by a recent IceCube study (57), based on stacking analyses of spatial correlations, that sets limits on the possible cumulative contribution of blazars in the second *Fermi*-LAT AGN catalog (*Fermi*-2LAC) to the diffuse TeV to PeV neutrino flux. The authors of this study concluded that, assuming a -2.5 power law index, blazars can contribute at most 27% (or, for a -2 index, at most 50%) of the total observed 10 TeV–2 PeV

neutrino flux, assuming complete oscillation between flavors. Neronov et al. (58) have obtained similar results.[4]

3.2. Galaxy Clusters/Groups and Associated Sources and Shocks

The importance of clusters of galaxies as amplifiers of the secondary radiation (neutrinos and γ-rays) from intracluster UHECR sources has been emphasized (e.g., 60, 61) because the CRs, after having been accelerated and undergone some secondary-producing $p\gamma$ or pp interactions inside their immediate source of origin (AGNs, supernovae, etc.), escape into the intracluster medium, which for large clusters of radius $R_{\rm cl} \sim$ few Mpc typically has an average gas density of $n_0 \sim 10^{-3}$ cm^{-3}, a magnetic field strength of $B_0 \sim 10^{-6}$ G, and a coherence length of $\ell_{\rm coh} \sim 30$ kpc. The typical diffusion coefficient $D(E_p) \propto E_p^{\alpha}$ [where $\alpha = (5/3, 1/2)$ for Komolgorov or Kraichnan turbulence spectra], and the diffusion time out of the cluster, $t_{\rm esc} \sim R_{\rm cl}^2/6D$, exceeds by orders of magnitude the light crossing time $R_{\rm cl}/c \sim 10$ My. During this diffusion time, the CRs' secondary-producing interactions greatly exceed those undergone in their original source. The interactions after the CRs escape into the IGM are typically less important than those undergone within a large cluster.

Accretion of external intergalactic gas onto the cluster gives rise to a stand-off shock, resulting in a shocked cluster gas layer and a stationary shock front facing the IGM. Such shocks can accelerate electrons to Lorentz factors $\gamma_e \sim 10^7$, which, as they scatter off microwave background photons, can contribute (62, 63) to the diffuse extragalactic γ-ray background. Cluster accretion shocks are also expected to accelerate CR protons (e.g., 64, 65), which undergo photohadronic or hadronuclear interactions and also contribute to the γ-ray background, as well as to a diffuse neutrino background (14, 31, 66). However, such cluster accretion shocks are in tension with clustering limits (13) and with radio limits (67).

Galaxy–galaxy collisions are also expected to occur in clusters of all sizes, as all galaxies are thought to have undergone at least one major merger (or, in the case of large galaxies, many) in their history, in typical hierarchical growth structure–formation schemes (e.g., 68). Single galaxies move in the cluster with virial velocities and shock-heat the intracluster gas; in addition, the gas in the colliding galaxy pairs undergoes strong shocks. The kinetic energy input rate is comparable to that of the accretion shock onto the cluster (69).

Fermi acceleration in these various types of shocks can lead to a power law energy distribution of CRs that are trapped in the cluster for a diffusion time that depends on the shocked layer width, magnetic field strength, and type of turbulence. For any such sources, the clusters act as CR reservoirs (61, 70, 71), allowing a longer time during which the CRs produce secondaries, mainly via pp interactions. This process leads to a neutrino spectrum whose slope mimics that of the protons and, assuming a slope of ~2–2.2, whose diffuse energy flux per energy decade $E_\nu^2 \Phi_{E_\nu}$ (e.g., 14, 69) is comparable to that of the first IceCube flux data in the sub-PeV to PeV range (2). One possibility that is allowed by the above-mentioned clustering and radio limits is that the CR acceleration occurs in AGNs in clusters and smaller groups of galaxies that serve as CR reservoirs (13), as the low-mass clusters can make a larger contribution. However, in all cases of optically thin sources (such as the above), proton slopes steeper than approximately -2.1 would result in violation of the Fermi limits (**Figure 2**). Here, the true diffuse isotropic γ-ray background should

[4]Resconi et al. (59) argue that, at the 3.3σ level, a bright (HBL) subclass of blazars could be responsible for some of the IceCube neutrinos as well as for UHECRs.

be interpreted as the fraction remaining after the resolved individual sources are subtracted and the contribution of unresolved sources is extrapolated (72).

Contributions to the diffuse secondary neutrino and γ-ray backgrounds from all models will be lower (71) if the accelerated UHECRs are predominantly heavy elements, as suggested by Auger observations (73, 74) at energies above $\sim 10^{18}$ eV. This is because the individual protons undergoing $p\gamma$ interactions carry only a fraction $1/Z$ of the total CR energy, and these heavier nuclei are subject to photodisintegration (e.g., 75).

3.3. Starburst Galaxies, Supernovae, and Hypernovae

Starburst galaxies (SBGs) are normal galaxies that are undergoing episodes of intense star formation, $\dot{M}_* \sim 1$–$10\, M_\odot\, \mathrm{year}^{-1}$, lasting 10^6–10^7 years. This is longer than the lifetime of young massive stars, which subsequently become supernovae (SNe). Normal galaxies typically undergo a number of star-forming episodes from birth, and the steady-state density of galaxies that at any time are starbursts is $n_{\mathrm{SBG}} \sim 3 \times 10^{-5}\, \mathrm{Mpc}^{-3}$, roughly two orders of magnitude less than that of quiescent galaxies. Approximately 20–30% of all star formation in the Universe occurred in such SBGs.

The radio luminosities of numerous SBGs with known redshift distances have been measured at 1.4 GHz, due to synchrotron radiation by relativistic electrons whose cooling time is shorter than the SBG phase lifetime. Thus, the energy production rate of electrons is a measure of the radio luminosity L_ω per unit frequency ω: $E_e^2 \mathrm{d}N_e/\mathrm{d}E_e \simeq 2\omega L_\omega$, where the factor 2 arises because the synchrotron frequency $\omega \propto E_e^2$. In quiescent galaxies such as ours, the ratio of energy input in CR protons to that in electrons is $\eta_{p/e} \sim 50$, but in SBGs, the increased SN activity and a magnetic field that is $\gtrsim 10^2$ times larger than that of the Milky Way are likely to result in a much slower diffusive escape of the CR protons (76), which can lose most of their energy in pp interactions, leading to pions. The luminosity per decade of ν_μ+anti-ν_μ is related to the photon luminosity ωL_ω by $E_\nu \mathrm{d}L_\nu = (1/3)\eta_{p/e} E_e^2 \mathrm{d}\dot{N}/\mathrm{d}E_e = (2/3)\eta_{p/e}\omega L_\omega$, where the factor 1/3 arises because 2/3 of the proton energy is carried by charged pions (1/3 by neutral pions); and because the charged pions decay into four particles ($\pi^+ \rightarrow \mu^+, \nu_\mu \rightarrow e^+, \nu_e, \nu_\mu$, anti-$\nu_\mu$), approximately half of the charged pions' energy is carried by muon neutrinos. Also, because the secondary electrons carry $\sim(2/3) \times 1/4 \sim 1/6$ of the proton energy, in SBGs one expects a CR proton to electron ratio of $\eta_{p/e} \sim 6$, so the muon neutrino luminosity per decade of energy is related to the photon luminosity per decade of frequency by $E_\nu \mathrm{d}L/\mathrm{d}E_\nu \simeq 4\omega L_\omega$, or $E_\nu^2(\mathrm{d}\dot{N}/\mathrm{d}E_\nu) \simeq 4E_\gamma^2(\mathrm{d}\dot{N}/\mathrm{d}E_\gamma)$. Thus, one can calibrate the CR luminosities of SBGs, or their expected neutrino energy flux, via their observed 1.4-GHz radio luminosities. A similar calibration can be also based on an established correlation of the infrared luminosity to the star-formation rate of SBGs. By analogy with our Galaxy's observed CR spectrum below the knee of $N_{\mathrm{obs}}(E_p) \propto E^{-2.75}$ and its confinement time $t_{\mathrm{esc}} \propto E^{-0.6}$, (76) one can assume a similar inferred injection spectrum $N(E_p) \propto E^{-2.15}$ for the SBGs. This spectrum predicts a well-motivated SBG neutrino diffuse flux (**Figure 5**) that is comparable to the Waxman–Bahcall (WB) flux (77). A flux of that order is indeed being observed by IceCube (2, 3), although so far there is no direct evidence linking it to SBGs.

SNe are the most likely ultimate sources responsible for accelerating the CRs in SBGs, which make many more SNe during their starburst phase than normal galaxies. A subclass of SNe termed hypernovae (HNe), which represent $\sim$5% of all SNe, are known to occur in all galaxies. Their ejecta velocities can reach semirelativistic values, as opposed to $v_{\mathrm{ej}} \sim 10^9\, \mathrm{cm\, s}^{-1}$ for normal SNe, and their ejecta kinetic energies (isotropic-equivalent value) can reach $\sim 10^{52}$ erg, as opposed to $\sim 10^{50}$–10^{51} erg for SNe. The maximum CR energy achievable by Fermi shock acceleration, according to Equation 9, is $E_{\mathrm{max}} \gtrsim 10^{15} Z$ eV for SNe and $E_{\mathrm{max}} \sim 10^{17} Z$ eV for HNe. These values were used (78, 79) to make source-specific neutrino background predictions before IceCube

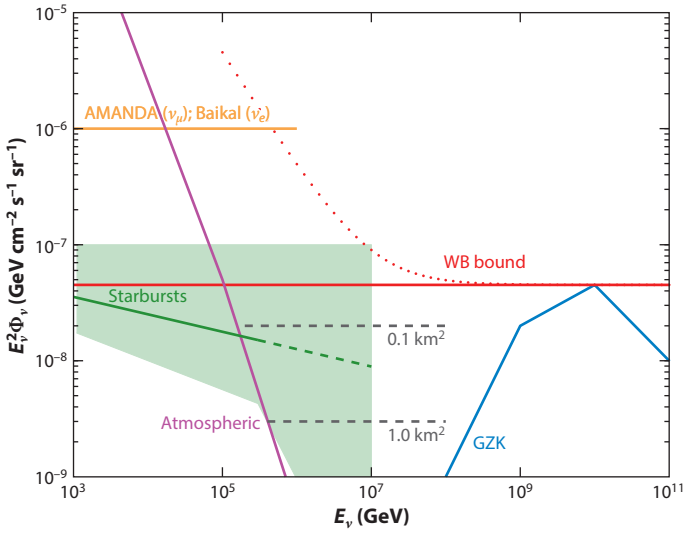

Figure 5

The possible starburst neutrino background (*shaded region*). The upper boundary is for a cosmic-ray index $s = 2$; the lower boundary is for $s = 2.25$ for $E_\nu < 10^{14.5}$ eV. The solid green line represents a slope $s = 2.15$. Also shown is the Waxman–Bahcall (WB) upper bound; the neutrino intensity expected from interaction with cosmic microwave background photons [Greisen–Zatsepin–Kuzmin (GZK)]; the atmospheric neutrino background; some experimental upper bounds from 2006, and the approximate sensitivity of 0.1-km^2 and 1-km^2 optical Cherenkov detectors. Modified from Reference 76.

observations were available, and subsequently, in light of both IceCube and *Fermi* data, numerous publications discussed HN neutrino production (e.g., 21, 22, 29, 80, 81). (Reference 23 provides a more detailed discussion of neutrino production and the constraints imposed by *Fermi* for both SNe and HNe in SBGs and star-forming galaxies, including the proton diffusion time in the host galaxy and host cluster during pp interactions.) These results indicate that SNe and HNe within $z \lesssim 4$ could provide, at most, 0.2–0.3 of the neutrino background without overproducing the observed γ-ray background. However, there are uncertainties in the star-formation rate at $z \gtrsim 2$ (e.g., 82), as well as in the ratio of HNe to SNe, both of which get worse at higher redshifts. By contrast, γ-rays from sources at redshifts $z \gtrsim 3$ undergo increasingly severe degradation due to an increase in $\gamma\gamma$ interactions in the increasingly dense intergalactic photon bath (40). Thus, the constraints from the *Fermi* observations can be satisfied (41) when one considers a significant contribution of SNe and HNe at $4 \lesssim z \lesssim 10$ from the earliest generations of stars (the so-called Population III stars). Of course, the apparent surface density of galaxies at high redshifts becomes very large, which makes it difficult to correlate any neutrino positions with candidate sources.

Reference 83 presents a discussion of the general conditions in SBGs and milder star-forming galaxies, including the star-formation rate, gas densities, magnetic fields, and dimensions. Note that, in some cases, the starburst phenomenon is suspected to have been initiated by a merger of two galaxies. In these cases, large-scale shocks would arise, which, as discussed in Section 3.2, would lead to CR acceleration and to secondary neutrinos and γ-rays. There are also systems in which an AGN and a starburst co-exist, and on the basis of SBG luminosity functions these could also be relevant for the neutrino background. Of course, starburst galaxy systems are also subject to the *Fermi*-imposed restriction requiring effective CR slopes flatter than approximately -2.2 (e.g., 13, 14).

3.4. Gamma-Ray Bursts

So-called classical GRBs have long been considered likely candidates for high-energy neutrino production (33). GRBs are catastrophic stellar events brought about by the core collapse of a massive star or the merger of a compact degenerate binary, leading to the most energetic explosions in the Universe. These explosions cause highly relativistic jets to emerge from the collapsing or merging progenitor system, with bulk Lorentz factors $\Gamma \sim 10^2$–10^3. In the case of core-collapse events (i.e., long GRBs, with MeV γ-rays lasting more than 2 s), sometimes an accompanying type Ic SN is also detected, in which the progenitor star's envelope is ejected.[5] GRBs are detected when a spacecraft such as *Swift* or *Fermi* triggers on an initial prompt GRB lasting milliseconds to tens of minutes, over the range of ~0.1–10 MeV, and sometimes up to ~100 GeV (e.g., 84, 85). The prompt emission is generally followed by a slowly decaying afterglow, which ranges from the X-ray to the optical to the radio range, over days to months. The photon spectra of both the prompt and afterglow emission appear nonthermal and have generally been ascribed (e.g., 85) to electron synchrotron and inverse Compton radiation. The prompt emission is typically modeled with Fermi acceleration in internal shocks inside the jet, whereas the afterglow arises from acceleration in an external shock, where the jet plows into the external medium. For the prompt emission, alternative mechanisms for the nonthermal emission have been proposed, including emission following reconnection or hadronic dissipation at a scattering photosphere, and emission from an intermediate zone due to shocks and magnetic reconnection or hadronic dissipation and reacceleration (e.g., 86–90). The acceleration of protons is expected to lead, via $p\gamma$ interactions in internal shocks, to TeV neutrinos (33) and, in external shocks, to EeV neutrinos (91). GeV neutrinos are also expected from proton acceleration and pp or $p\gamma$ interactions in photospheres (92–95), and up to multi-TeV neutrinos can be produced in intermediate magnetic or hadronic dissipation zones (90, 96, 97).

The initial IceCube test of GRB neutrino models derived upper limits from the initial 40-string and 52-string arrays (99–101) by comparing them with a simplified internal shock model with an unchanging radius parameterized by the total γ-ray energy, Lorentz factor Γ, outflow time variability t_v, and a standardized broken power law photon spectrum; using the Δ resonance approximation for the photohadronic interaction; and assuming a CR baryon loading (relativistic proton to electron ratio) of $f_p = L_p/L_e$. This initial study concluded that for $f_p = f_e^{-1} = L_p/L_e = 10$, this model overpredicted the data by a factor of five, and a model-independent analysis comparing the observed diffuse neutrino flux with the expected flux also yielded negative results. This important early result from IceCube demonstrated the ability of this major new Cherenkov neutrino facility to test astrophysical models. Subsequently, by using the same internal shock model but correcting various approximations and including multipion and kaon channels, as well as interactions with the entire target photon spectrum (102–104), researchers calculated lower model fluxes that did not disagree with the 40-string and 56-string data. Interestingly, the original approximate internal shock calculation (33) also resulted in a lower flux that was a factor of 10 lower than the WB bound and within the above IceCube limit.

Much more extensive tests of GRB prompt emission models were performed against a set of more accurate internal shock models, as well as a magnetic dissipation model (ICMART) (89) and a baryonic photospheric model (93, 97), assuming steady-state, fixed-radius emission zones. These statistical tests involved 4 years of IceCube data, including 2 years of data from the full array (98). The authors of these studies concluded (**Figure 6**) that, at the 99% confidence level, less than 1% of the observed diffuse neutrino background is contributed by the observed sample of 592

[5]However, only a very small fraction of all type Ic SNe are associated with GRBs.

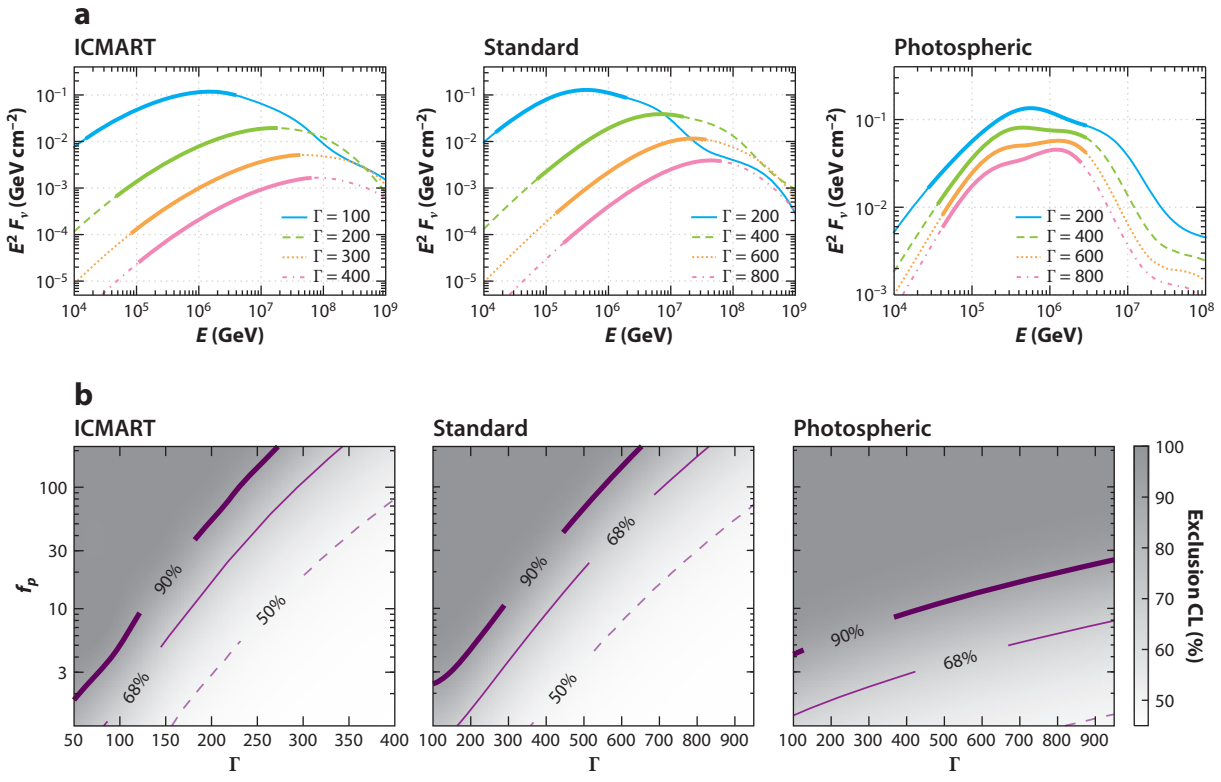

Figure 6

(*a*) Total normalized neutrino fluxes for (*from left to right*) ICMART, internal shock, and (baryonic) photospheric models for various Lorentz factors Γ, scaling with f_p (here, 10). (*b*) Allowed region for f_p and Γ for the different models. Modified from Reference 98.

EM-detected GRBs. If the basic acceleration paradigm used for the emission zones is correct, and this result continues to stand, then it would indicate the ratio $f_p = L_p/L_e \lesssim 1$ in such models. Other photospheric models that have substantially different neutrino production physics (94, 105) or include time dependence (96) may avoid these restrictions, but so far these models have been only qualitatively compared with the data.

The classical GRBs discussed above are typically bright and are EM-detected by spacecraft at an observed rate of $\sim$300 year^{-1}, or $\sim$700 year^{-1} when corrected for viewing constraints; the total sample is in the thousands. There are, however, other known or suspected types of GRBs, as discussed in the following section.

3.5. Low-Luminosity, Shock-Breakout, and Choked Gamma-Ray Bursts

Although low-luminosity GRBs (LLGRBs) have been observed for a long time, only a few are known, all of which were detected at very close distances $z \ll 1$ due to their intrinsic EM dimness.[6] LLGRBs appear to form a distinct class, although, aside from their low luminosity, they share

[6]By contrast, classical high-luminosity GRBs have been detected in the $0.5 \lesssim z \lesssim 9$ range.

many characteristics of classical long GRBs, such as a nonthermal (albeit softer) spectrum that may be related to a relativistic jet emerging from a collapsing stellar progenitor. An SN ejecta, being nearby, is generally detected as well and appears to be semirelativistic (e.g., 106, 107). However, the local occurrence of LLGRBs per unit volume rate is an order of magnitude higher than for classical GRBs (e.g., 108). The neutrino luminosity of the classical GRB internal shock model suggests that LLGRBs could contribute significantly to the diffuse neutrino background (109, 110).

Shock-breakout GRBs, of which even fewer have been detected, also show a soft, low-luminosity GRB and/or X-ray burst (e.g., 107), followed by a brightening of ultraviolet and later optical radiation, which resembles the brightening of an SN but with certain distinct characteristics. This phenomenon is thought to involve a jet that emanated from the core of a collapsing massive star, as for classical long GRBs, but that had less momentum and just barely managed to break out from the star. As the jet propagated it imparted extra energy to the expanding stellar envelope, and the boosted SN shock appears to break out (i.e., the photon diffusion time becomes shorter than the expansion time) in the dense wind that precedes the ejecta (111, 112).

Choked GRBs, which were thought to exist (113) prior to the discovery of shock breakouts and extragalactic neutrinos, are core-collapse objects in which the jets did not emerge, either because they did not have enough momentum or because they were not powered long enough to reach the outer radius of the stellar envelope. Internal or recollimation shocks (or magnetic dissipation) in such stalled, buried jets could accelerate protons, leading to GeV neutrinos, whereas the γ-rays would be thermalized, and only a subsequent optical SN would be expected (which, at redshifts $z \gtrsim 1$, is rarely detectable). So far, searches performed with IceCube have not yielded any candidates (114). Alternatively, if the jet was energetic enough to eventually emerge, before doing so the pre-emergence jet could again undergo shocks or dissipation, giving rise to a neutrino precursor followed by a successful GRB, which could be an LLGRB or a classical GRB, as opposed to a failed (choked) GRB (113). Shock breakouts represent an intermediate case between the choked and the emergent GRBs. A unified picture of the expected EM properties of all three cases is presented elsewhere (115).

All three types of LLGRBs (**Figure 7**) are expected to be "hidden" neutrino sources, given that either their EM emission is so weak that only the very few nearest cases trigger a γ-ray detector or their EM luminosity is a protracted SN-like event in the optical/infrared range; because such events are typically at very high redshifts, they are, again, hard to detect. Both analytical and (in some cases) numerical calculations of the high-energy neutrino spectral fluences have been

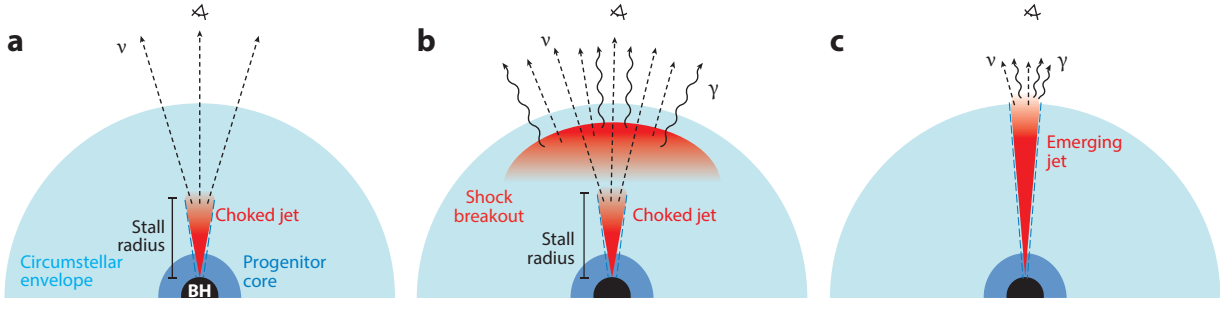

Figure 7

Possible scenarios for jet and stellar envelope interaction in a core collapse. (*a*) Choked jet and orphan neutrinos. (*b*) Precursor neutrinos and shock breakout. (*c*) Low-luminosity emergent jet γ-ray burst. Modified from Reference 35.

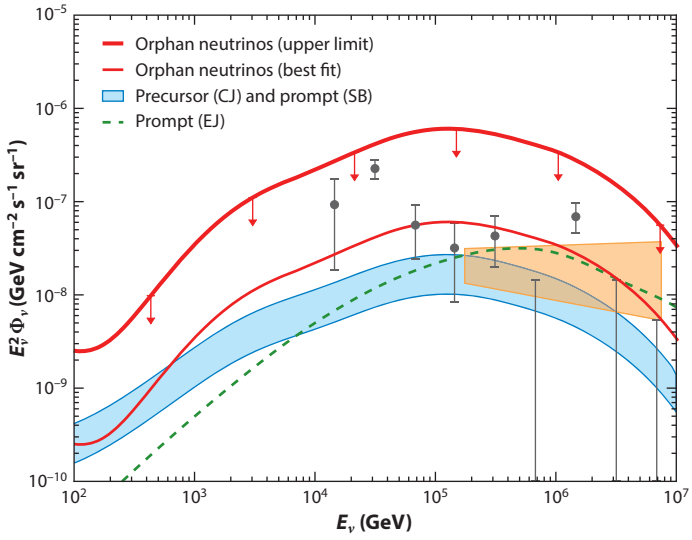

Figure 8

Predicted all-flavor diffuse neutrino fluxes from three types of low-luminosity γ-ray bursts (LLGRBs): choked jets (CJ; orphan neutrinos) (*thick red line*); precursor and shock-breakout neutrinos (SB) (*blue region*); and prompt emergent jet neutrinos (EJ) (*dashed line*). The data points are based on the IceCube combined analysis (9), and the orange shaded region is an estimate based on IceCube talks on the upgoing muon analysis. Modified from Reference 35.

performed separately for choked jet GRBs (34, 116–121), shock-breakout GRBs (122–124), and LLGRBs (109, 125).

More recently, a unified calculation and a comparison of all three types of hidden GRBs were performed (**Figure 8**) (35). The calculation used a standard GRB luminosity function, and neutrino emission was considered only from choked or precursor jets whose luminosity was low enough to ensure that the buried shocks were not radiation broadened (because buried jets exist at lower radii and their radiation density is comparatively higher than in emergent jets). This ensures a collisionless shock, in which the particles scattered between pre- and postshock regions are subjected to the full bulk velocity difference, as needed for first-order Fermi acceleration. Otherwise, for higher-luminosity buried jets, the photon mean-free path governs the shock width, which becomes larger than the typical photon mean-free path or gyroradius; the scattered particles are not exposed to the full bulk velocity difference, and classical first-order Fermi acceleration is not expected (e.g., 34, 126). Low-power jets are also required in order for the jet to stall before it emerges from the star (34, 35). The conclusion from this calculation (35) is that a combination of choked jet GRBs, shock-breakout GRBs, and LLGRBs could in principle provide the observed IceCube neutrino flux without violating either the *Fermi* observations or the (classical GRB) stacked neutrino analyses.

3.6. Other Sources: Tidal Disruption Events and White Dwarf Mergers

Occasionally, tidal disruption events (TDEs) of stars by MBHs at the centers of some galaxies can also give rise to relativistic jets, as in the γ-ray source Sw J1644+57 (127). If such a TDE occurs in a galaxy whose bulge gas density is high enough, or if the TDE initially leads to a precursor wind before the jet is produced (e.g., 128), then this external gas may either choke the jet or lead to a

shock breakout similar to that in GRBs (e.g., 37). The rates are highly uncertain, but a fraction of observed VHE neutrinos may arise from such events, whose γ-rays could be effectively EM hidden because of the high optical depth of the enshrouding gas (for some recent calculations, see, e.g., References 38, 129, and 130).

White dwarf (WD) mergers are another possible type of hidden neutrino source. WDs are left over at the end of the evolution of stars with low to intermediate masses (lighter than those producing core-collapse SNe), and WD binaries are abundant enough that their merger rate is estimated to be comparable to that of type Ia SNe. Such WD mergers may lead to a magnetized outflow (131), in which photons are trapped up to the diffusion radius, where the diffusion time is equal to the dynamic time. Magnetic reconnection in the flow beyond the diffusion radius can lead to proton acceleration, which gives rise to pp interactions that result in secondary neutrinos and γ-rays (36). Because the scattering optical depth is still large at the diffusion radius, the γ-rays are degraded and these sources are effectively dark, or at least considerably dimmed, as far as the *Fermi* energy sensitivity range is concerned, thus avoiding the Fermi constraint. The neutrino flux may be a substantial fraction of the IceCube flux, depending on model uncertainties and WD merger rates.

Other stellar sources in starburst galaxies have been considered as the means for producing VHE neutrinos. These include magnetars, young pulsars, and macronovae, which are not covered in this review.

4. DISCUSSION

The discovery of extragalactic VHE neutrinos by IceCube has opened up an entirely new realm of possibilities for exploring the physics of the highest-energy astrophysical sources, potentially out to the furthest reaches of the Universe. However, so far the small number of events at these energies has allowed us to address only the aggregate emission in the form of a diffuse background radiation. The identity and nature of the sources remain unknown; however, we expect significant progress in this area with multimessenger approaches, such as the AMON project (132, 133) and others, especially those combining the detection of neutrinos with their (relatively) more easily detectable EM counterparts.

Accumulating high-energy neutrino and γ-ray data will make it increasingly feasible to draw general conclusions about the physical mechanisms producing the neutrinos, as well as about the general environment in which they originate and in which their secondaries propagate (e.g., 9). Furthermore, these neutrinos and their coproduced γ-rays must be linked to high-energy CRs with energy in the 10^{14}–10^{17}-eV range, and possibly beyond. The fact that the IceCube neutrino emission level is close to the WB limit (77) has provided the motivation for an interesting argument (134) indicating that the input of CRs' energy per decade over their entire spectral range may be approximately constant at the level of $\sim 10^{44}$ erg Mpc^{-3} year^{-1}; their manifestation in the IceCube range would be the observed neutrinos (e.g., 13, 135).

Further progress can be expected with the future completion of the KM3NeT underwater neutrino detector in the Mediterranean Sea (136). The capabilities of KM3NeT will be roughly similar to those of IceCube, and it will have a complementary Northern Hemisphere location. Both IceCube (137) and KM3NeT (136) have proposed extending their sensitivity to lower and higher energies, which could address interesting questions concerning fundamental physics (e.g., 138) and dark matter (139, 140). Detectors with much larger effective areas, such as the ANITA balloon telescope (e.g., 141), the proposed very large radio arrays in Antarctica such as ARIANNA (142) and ARA (143), and space-based detectors such as JEM-EUSO (144), will extend the sensitivity to the very low fluxes expected at energies in the 10^{20}–10^{21} eV range and above. This will allow

researchers to address important questions concerning cosmogenic neutrino production, including performing tests for the presence of UHECRs at or beyond the Greisen–Zatsepin–Kuzmin (GZK) radius ∼100 Mpc, determining whether the spectrum extends beyond the GZK energy of $\sim 6 \times 10^{19}$ eV, constraining the heavy-element content, and so forth. The completion of the approved CTA (Cherenkov Telescope Array), a large, ground-based VHE γ-ray detector (e.g., 145), will also be extremely useful for simultaneous neutrino and γ-ray detection, localization, and source characterization.

5. APPENDIX

5.1. Neutrino Production Mechanisms

Aside from the possibility of high-energy ($\gtrsim$GeV) neutrinos being produced by the decay of exotic (beyond-the-Standard-Model) particles, such neutrinos are expected to be produced in astrophysical scenarios. CRs can lead, via hadronic interactions such as pp, pn, or $p\gamma$, to the production of mesons, mainly charged and neutral pions, which decay as, for instance, $\pi^+ \to \mu^+ \nu_\mu$ followed by $\mu^+ \to e^+ \nu_e \text{anti-}\nu_\mu$ or $\pi^0 \to 2\gamma$. For proton (or neutron) CRs, the energy of the decay neutrino is typically related to the parent CR proton or neutron energy by $\varepsilon_\nu \simeq 0.04$–$0.05 \varepsilon_{p,n}$. For a total CR (proton) volumetric energy generation rate Q_p (erg Gpc^{-3} year^{-1}), leading to a CR energy generation rate per decade of $\varepsilon_p Q_{\varepsilon_p}$, one expects an all-flavor neutrino energy generation rate per decade of energy of

$$\varepsilon_\nu Q_{\varepsilon_\nu} \approx \frac{K}{(1+K)} \left(\frac{3}{4}\right) \min[1, f_{p\gamma/pp}] \varepsilon_p Q_{\varepsilon_p}, \quad 1.$$

where ε_j denotes the source-frame energy of particles of type j. Here the factor 3/4 enters because approximately 1/4 of the energy in the decay chain is lost to $e^\pm$, which end up going into photons; and K is the average number ratio of charged to neutral pions, which is $K \simeq 1$ for the $p\gamma$ and $K \simeq 2$ for pp and pn processes. The factor $\min[1, f_{p\gamma/pp}]$ is the pp or $p\gamma$ meson production efficiency,

$$f_{p\gamma/pp} \simeq n_{\gamma/p} \kappa_p \sigma^{\rm incl}_{p\gamma/pp} c t_{\rm int}, \quad 2.$$

where $n_{\gamma/p}$ is the number density of the target photons (protons); κ_p is the inelasticity (i.e., the relative energy loss per interaction, $\Delta\varepsilon_p/\varepsilon_p$), which on average is $\kappa_p \simeq 0.5$ for both pp and $p\gamma$; the inclusive (i.e., total) cross section is $\sigma^{\rm incl}_{p\gamma} \simeq 5 \times 10^{-28}$ cm^2 for $p\gamma$ or $\sigma^{\rm incl}_{pp} \simeq 8 \times 10^{-26}$ cm^2 for pp; and $t_{\rm int}$ is the time available for interactions, with $c t_{\rm int}$ the interaction length. The interaction time is generally $t_{\rm int} = \min[t_{\rm inj}, t_{\rm esc}, t_H]$, where $t_{\rm inj}$ is the CR injection time, $t_{\rm esc}$ is the CR escape time from the interaction region, t_H is the local Hubble time or age of the Universe in the source frame, and the interaction length is along a random walk path between interactions.

The neutral pions result in an accompanying γ-ray emission, $\pi^0 \to 2\gamma$, which is related (at the source) to the neutrino emission by

$$\varepsilon_\gamma Q_{\varepsilon_\gamma} \approx \frac{1}{K} \frac{4}{3} \left(\varepsilon_p Q_{\varepsilon_p}\right)|_{\varepsilon_\nu = \varepsilon_\gamma/2}, \quad 3.$$

where the energy of the γ-rays is, on average, $\varepsilon_\gamma \simeq 2\varepsilon_\nu$.

If we denote with E_j the energies of particles j observed at Earth, the neutrinos observed by IceCube from a source at redshift z are related to the parent proton energy by

$$E_\nu \sim 0.05 E_p \simeq 2\, \varepsilon_{p.17}\, [2/(1+z)] \text{ PeV}, \quad 4.$$

and the all-flavor diffuse neutrino flux Φ_ν per steradian with observed energy E_ν at Earth is

$$E_\nu^2 \Phi_\nu = \frac{c}{4\pi} \int \frac{dz}{(1+z)^2 H(z)} \left[\varepsilon_\nu Q_\nu\right]|_{\varepsilon_\nu=(1+z)E_\nu}, \quad 5.$$

in units of, for instance, $\mathrm{GeV\,cm^{-2}\,s^{-1}\,sr^{-1}}$. Here, $H(z) \simeq H_0 \left[\Omega_V + (1+z)^3 \Omega_M\right]^{1/2}$ is the redshift-dependent Hubble parameter, where $H_0 \simeq 70$ km $\mathrm{s^{-1}\,Mpc^{-1}}$. For a local ($z = 0$) CR proton differential energy input rate Q_{E_p}, the diffuse neutrino background per flavor at Earth (which follows from Equation 5) is approximately (e.g., 14, 33)

$$E_\nu^2 \Phi_\nu \approx \frac{c\, t_H\, \xi_z}{4\pi} \left[\frac{K}{4(1+K)}\right] \min[1, f_{p\gamma/pp}] \left(E_p\, Q_{E_p}\right), \quad 6.$$

where the per flavor factor is $[K/4(1+K)] = [1/8,\ 1/6]$, that is, 1/8 for $p\gamma$ ($K = 1$) or 1/6 for pp ($K = 2$); $t_H \simeq 13.2$ Gyr; and ξ_z is a redshift evolution factor that, for sources evolving approximately as the star-formation rate, such as GRBs or SNe, is $\xi_z \sim 3$ at $z \sim 1$. The corresponding diffuse γ-ray background associated with Equation 6, in the absence of EM cascades, is given by

$$E_\gamma^2 \Phi_\gamma \approx 2 \left(E_\nu^2 \Phi_\nu\right)|_{E_\nu = 0.5 E_\gamma}. \quad 7.$$

5.2. Cosmic-Ray Acceleration Mechanisms

The photons or hadrons entering the interactions of $p\gamma$, pp, pn, and so forth must have energies such that the center-of-momentum energy is above the threshold for the production of pions or other mesons. Thus, either the photons involved in $p\gamma$ must have high lab-frame energies or the hadrons initiating the pp or $p\gamma$ interactions must be highly relativistic; in other words, they must be CRs. Among the most promising mechanisms to explain CR acceleration are diffusive shock acceleration (DSA) and magnetic reconnection acceleration, both of which are first-order Fermi-type mechanisms; stochastic or turbulent acceleration, which is a second-order Fermi-type mechanism; and electrostatic-type acceleration mechanisms, such as pulsar magnetospheric acceleration or wake field acceleration.

The DSA mechanism can arise in systems in which a strong shock propagates, with charged particles scattering back and forth across the shock interface. Typically such shocks are collisionless—that is, the binary particle collision mean-free path is very large compared with that for scattering by magnetic irregularities. For a subrelativistic (or mildly relativistic) shock propagating into a stationary upstream medium, a proton that is already relativistic in the downstream (moving) region can run ahead of the shock and will be randomized by scattering against magnetic irregularities in the upstream region. The particle is then overtaken by the shock and finds itself again in the downstream region, where it is again randomized by magnetic irregularities. The process then repeats itself, and at each step of the cycle the particle gains energy at the expense of the upstream–downstream gas relative bulk velocity difference. Each time the particle is hit head on, the net relative energy boost is $\Delta E/E \propto (v_s/c)$ (and hence first order), where v_s is the shock velocity.[7]

In such first-order shock acceleration scenarios, the typical acceleration timescale is

$$t_{\rm ac}^{\rm dsa} \simeq \eta \left(\frac{r_{\rm L}}{c}\right) \beta_s^{-2}, \quad 8.$$

where $r_{\rm L} = E/Z_e B$ is the Larmor radius, Z_e is the particle charge, B is the magnetic field, $\beta_s = v_s/c$ is the shock velocity in the upstream frame, and $\eta \sim 1$–10. This acceleration timescale is

[7]Note that the initial particles injected must already be at least mildly relativistic and that for relativistic shocks the treatment is more complicated after the first scattering, but under some approximations qualitatively similar results are expected.

on the order of the gyration time, as it is proportional to the maximum particle energy ε reached and is controlled by the spatial diffusion time. If the shocks occur in a jet oriented toward the observer with a bulk Lorentz factor Γ, the acceleration time, Larmor radius, magnetic field, and shock velocity in Equation 8 should be interpreted as the corresponding quantities in the jet frame, namely $t'_{\rm ac}$, $r'_{\rm L}$, B', and β'_s. A limit on the maximum energy is imposed by requiring that $t_{\rm ac}$ not exceed the dynamic time, which in the nonrelativistic case is $t_{\rm dyn} \simeq R/v_s$, where R is the lab-frame dimension of the acceleration region (e.g., radius of shock):

$$E_{\rm max} \simeq \left(\frac{\beta_s}{\eta}\right)\frac{Z_e BR}{(1+z)}. \qquad 9.$$

Here, z is the redshift of the source.[8] This criterion is equivalent to the confinement criterion that $r_{\rm L}$ be smaller than the acceleration region R. For shocks in a jet with bulk Lorentz factor Γ, in the comoving frame $t'_{\rm dyn} \simeq R/c\,\Gamma$, so $(20\eta/3)(r'_{\rm L}/c)\beta_s'^{-2} \leq (R/c\,\Gamma)$ leads to a lab-frame maximum energy given by Equation 9, but with β_s replaced by $\beta'_s \to 1$ and B replaced by B', the comoving field. Alternatively, the maximum energy may be limited by the requirement that the acceleration time be shorter than the synchrotron radiation loss time of the accelerated particle.

Magnetic reconnection is another acceleration process that operates as a Fermi first-order mechanism. Long considered to be the cause of particle acceleration in solar flares, magnetic reconnection is expected to be ubiquitous in many astrophysical situations in which shear, turbulence, or rotation leads to reconnection. In addition to flares, candidate sites include azimuthally sheared accretion disks, transverse shear between jets and the environment, and magnetohydrodynamic (MHD) turbulent media, among others. A schematic X-point geometry considers regions of dimension $\ell_{\rm rec}$ of opposite magnetic polarities that approach each other, for instance, along the $\pm y$ direction, at a subrelativistic speed $\beta_{\rm rec} \lesssim 0.1$, leading to a thin reconnection layer with an electric field along the x axis, where plasma flows out along the $\pm x$ direction at the Alfvén speed $v_{\rm A} \sim 1$. Charged particles rotate repeatedly in and out of the opposite converging regions under the action of the opposing magnetic field polarities while experiencing a net acceleration along the x axis under the effect of the reconnection layer's electric field. A simple but illustrative calculation (146) shows that the effective acceleration timescale is $t_{\rm ac}^{\rm rec} \simeq [2\pi/(1-1/A)](r_{\rm L}/c) \sim 4\pi(r_{\rm L}/c)$, where for reasonable reconnection rates $A \sim 2$, yielding an acceleration timescale that is essentially Equation 8 for the diffusive shock acceleration (i.e., roughly the gyration period). The maximum particle energy is obtained by equating the acceleration time to the dynamic time, which leads approximately to Equation 9, or by equating the acceleration time to the radiation loss time.

Stochastic acceleration, such as that expected in MHD turbulent media as particles are scattered by waves of velocity v_w with random orientations, leads to relative energy changes that are second order, $\propto (v_w/c)^2$, because the particles experience both head-on and overtaking collisions with the waves. This is a process of diffusion in energy space; the particles sometimes gain and sometimes lose energy, and the first-order energy changes cancel out, resulting in a net average energy gain. For magnetic field fluctuations with a spectral energy density of $W_k \propto k^{-q}$ (where k is the wave number corresponding to turbulent length scales $\ell \sim 2\pi/k$), for resonant scattering (where $r_{\rm L} \sim k$), one expects an energy diffusion coefficient $D_{\varepsilon\varepsilon} \propto \varepsilon^q$ and a scattering and acceleration time

[8] More exactly, if the minimum spatial diffusion coefficient in the Bohm limit is $D_{\rm min} = \eta' r_{\rm L} c/3$, then $t_{\rm ac}^{\rm dsa} \simeq (20\eta'/3)(r_{\rm L}/c)\beta_s^{-2}$, and $\varepsilon_{\rm max} \simeq (3\beta_s/20\eta')Z_e BR/(1+z)$.

$t_{\rm ac} \propto \varepsilon^{2-q}$:

$$t_{\rm ac}^{\rm sto} \simeq \frac{\varepsilon^2}{4D_{\varepsilon\varepsilon}} \sim \eta_{\rm sto}\frac{\ell_t}{c}\left(\frac{r_{\rm L}}{\ell_t}\right)^{2-q}. \qquad 10.$$

Here, $\ell_t \sim 2\pi/k_{\rm min}$ and $\eta_{\rm sto} \sim 1$ (e.g., 147–149). This timescale is generally longer than that of Equation 8 for shock acceleration but is still shorter than the MHD wave timescale ℓ_t/c, so it can act as a slow-heating mechanism on a subhydrodynamical timescale (90, 148). At the highest energies, where $r_{\rm L} \sim \ell_t$, or for values of $q = 2$, as suggested by various MHD turbulence simulations, the energy diffusion coefficient becomes $D_{\varepsilon\varepsilon} \propto \varepsilon^2$ (150), and the stochastic timescale becomes comparable to Equation 8 for shock acceleration. If we equate the acceleration time (10) to the hydrodynamic time $R/c\beta\Gamma$ (or $R/u = R/c\beta$ in the nonrelativistic case), the lab-frame maximum energy is

$$E_{\rm max} \simeq Z_e B\ell_t \times \begin{cases} 1 & \text{for} \quad q = 2, \\ (R/\eta\beta\Gamma\ell_t)^{1/(2-q)} & \text{for} \quad q \neq 2, \end{cases} \qquad 11.$$

where for a jet the comoving B' value should be used.

SUMMARY POINTS

1. Extragalactic neutrinos in the TeV to PeV range have been discovered, introducing a completely new channel for studying VHE cosmic physical processes at the highest redshifts in the Universe.
2. These neutrinos provide important clues for investigating the origin of high-energy CRs, and they provide stringent constraints on the possible source models being considered.
3. So far, a smoking-gun identification of the actual sources has remained elusive because the angular accuracy of the arrival directions of individual neutrinos remains on the order of a degree or larger.
4. Co-emitted γ-rays, when detected, are likely to help address this problem, as will statistical analyses based on larger numbers of neutrinos and more complete candidate source catalogs.
5. We live in an exciting new era in which tremendous progress is being made.

FUTURE ISSUES

1. The main desiderata for future advances will be to achieve significantly higher event statistics, which will require, for example, the approval and building of the second-generation extensions to IceCube, the completion of new facilities such as KM3NeT, and the expansion of multimessenger localization operations such as AMON.
2. These sensitivity increases will also be crucial for investigating pressing issues of basic neutrino physics, for dark matter searches, and for other beyond-the-Standard-Model questions.

3. A major problem is that the observed diffuse neutrino background flux appears to overpredict the observed diffuse γ-ray flux, assuming the "usual suspect," namely optically thin candidate sources.
4. Unless otherwise resolved, this issue is suggestive of EM-hidden sources, namely sources where γ-rays are absorbed or degraded. Possibilities being considered are buried LLGRB jets or tidal disruption jets, among others, but much more research remains to be done.
5. Many new surprises can be expected from the major new facilities coming online in the next decade.

DISCLOSURE STATEMENT

The author is not aware of any affiliations, memberships, funding, or financial holdings that might be perceived as affecting the objectivity of this review.

ACKNOWLEDGMENTS

The author is grateful to Douglas Cowen, Kohta Murase, and Marek Kowalski for useful communications and to NASA (NNX13AH50G) for partial support.

LITERATURE CITED

1. Aartsen MG, et al. *Phys. Rev. Lett.* 111:021103 (2013)
2. IceCube Collab. *Science* 342:1242856 (2013)
3. Aartsen MG, et al. *Phys. Rev. D* 91:022001 (2015)
4. Gaisser T, Halzen F. *Annu. Rev. Nucl. Part. Sci.* 64:101 (2014)
5. Babson J, et al. *Phys. Rev. D* 42:3613 (1990)
6. Avrorin AD, et al. *Eur. Phys. J. Web Conf.* 116:1105 (2016)
7. Margiotta A. (ANTARES Collab.) *J. Phys. Conf. Ser.* 718:062041 (2016)
8. Kowalski M. In *Proceedings of the 27th International Conference on Neutrino Physics and Astrophysics* (*Neutrino2016*). Bristol, UK: IOP. In press (2017)
9. Aartsen MG, et al. *Astrophys. J.* 809:98 (2015)
10. Aartsen MG, et al. *Phys. Rev. Lett.* 114:171102 (2015)
11. IceCube Collab., et al. arXiv:1609.04981 [astro-ph] (2016)
12. IceCube Collab., Pierre Auger Collab., Telescope Array Collab. *J. Cosmol. Astropart. Phys.* 1:037 (2016)
13. Murase K, Waxman E. arXiv:1607.01601 [astro-ph] (2016)
14. Murase K, Ahlers M, Lacki BC. *Phys. Rev. D* 88:121301 (2013)
15. Anchordoqui LA, et al. arXiv:1306.5021 [astro-ph] (2013)
16. Barger V, et al. arXiv:1407.3255 [astro-ph] (2014)
17. Kistler MD, Laha R. arXiv:1605.08781 [astro-ph] (2016)
18. Sahu S, Zhang B. arXiv:1612.09043 [hep-ph] (2016)
19. Anchordoqui LA, et al. arXiv:1611.07905 [astro-ph] (2016)
20. Biehl D, et al. arXiv:1611.07983 [astro-ph] (2016)
21. He HN, et al. *Phys. Rev. D* 87:063011 (2013)
22. Liu RY, et al. *Phys. Rev. D* 89:083004 (2014)
23. Senno N, et al. *Astrophys. J.* 806:24 (2015)
24. Murase K. *AIP Conf. Proc.* 1666:040006 (2015)
25. Ahlers M. *eConf* C14102.1. 8 pp. (2015)
26. Berezinskii VS, Smirnov AI. *Astrophys. Space Sci.* 32:461 (1975)

27. Ackermann M, et al. *Astrophys. J.* 799:86 (2015)
28. Liu RY, et al. *Phys. Rev. D* 89:083004 (2014)
29. Chang XC, Wang XY. *Astrophys. J.* 793:131 (2014)
30. Ando S, Tamborra I, Zandanel F. *Phys. Rev. Lett.* 115:221101 (2015)
31. Zandanel F, Tamborra I, Gabici S, Ando S. *Astron. Astrophys.* 578:A32 (2015)
32. Murase K, Guetta D, Ahlers M. *Phys. Rev. Lett.* 116:071101 (2016)
33. Waxman E, Bahcall J. *Phys. Rev. Lett.* 78:2292 (1997)
34. Murase K, Ioka K. *Phys. Rev. Lett.* 111:121102 (2013)
35. Senno N, Murase K, Mészáros P. *Phys. Rev. D* 93:083003 (2016)
36. Xiao D, Mészáros P, Murase K, Dai ZG. arXiv:1608.08150 [astro-ph] (2016)
37. Wang XY, Liu RY. arXiv:1512.08596 [astro-ph] (2015)
38. Senno N, Murase K, Meszaros P. arXiv:1612.00918 [astro-ph] (2016)
39. Kimura SS, Murase K, Toma K. *Astrophys. J.* 806:159 (2015)
40. Chang XC, Liu RY, Wang XY. *Astrophys. J.* 825:148 (2016)
41. Xiao D, Mészáros P, Murase K, Dai ZG. *Astrophys. J.* 826:133 (2016)
42. Dennison CD, Giebels B. arXiv:1602.06592 [astro-ph] (2016)
43. Protheroe RJ, Kazanas D. *Astrophys. J.* 265:620 (1983)
44. Biermann PL, Strittmatter PA. *Astrophys. J.* 322:643 (1987)
45. Stecker FW, Salamon MH. *Space Sci. Rev.* 75:341 (1996)
46. Atoyan A, Dermer CD. *Phys. Rev. Lett.* 87:221102 (2001)
47. Murase K, Inoue Y, Dermer CD. *Phys. Rev. D* 90:023007 (2014)
48. Padovani P, et al. *Mon. Not. R. Astron. Soc.* 457:3582 (2016)
49. Alvarez-Muñiz J, Mészáros P. *Phys. Rev. D* 70:123001 (2004)
50. Pe'er A, Murase K, Mészáros P. *Phys. Rev. D* 80:123018 (2009)
51. Murase K. arXiv:1511.01590 [astro-ph] (2015)
52. Dermer CD, Murase K, Inoue Y. *J. High Energy Astrophys.* 3:29 (2014)
53. Padovani P, Petropoulou M, Giommi P, Resconi E. *Mon. Not. R. Astron. Soc.* 452:1877 (2015)
54. Stecker FW. *Phys. Rev. D* 88:047301 (2013)
55. Becker Tjus J, et al. *Phys. Rev. D* 89:123005 (2014)
56. Hooper D. *J. Cosmol. Astropart. Phys.* 09:002 (2016)
57. IceCube Collab., et al. arXiv:1611.03874 [astro-ph] (2016)
58. Neronov A, Semikoz DV, Ptitsyna K. arXiv:1611.06338 [astro-ph] (2016)
59. Resconi E, et al. arXiv:1611.06022 [astro-ph] (2016)
60. Völk HJ, Aharonian FA, Breitschwerdt D. *Space Sci. Rev.* 75:279 (1996)
61. Berezinsky VS, Blasi P, Ptuskin VS. *Astrophys. J.* 487:529 (1997)
62. Loeb A, Waxman E. *Nature* 405:156 (2000)
63. Keshet U, et al. *Astrophys. J.* 585:128 (2003)
64. Norman CA, Melrose DB, Achterberg A. *Astrophys. J.* 454:60 (1995)
65. Inoue S, Aharonian FA, Sugiyama N. *Astrophys. J. Lett.* 628:L9 (2005)
66. Murase K, Inoue S, Nagataki S. *Astrophys. J. Lett.* 689:L105 (2008)
67. Zandanel F, Pfrommer C, Prada F. *Mon. Not. R. Astron. Soc.* 438:124 (2014)
68. Nelson D, et al. *Astron. Comput.* 13:12 (2015)
69. Kashiyama K, Mészáros P. *Astrophys. J. Lett.* 790:L14 (2014)
70. Murase K, Inoue S, Nagataki S. *Astrophys. J. Lett.* 689:L105 (2008)
71. Kotera K, et al. *Astrophys. J.* 707:370 (2009)
72. Ackermann M. (Fermi Collab.) *Phys. Rev. Lett.* 116:151105 (2016)
73. Watson A. arXiv:1610.09098 [astro-ph] (2016)
74. Pierre Auger Collab., et al. arXiv:1609.08567 [astro-ph] (2016)
75. Allard D, et al. *J. Cosmol. Astropart. Phys.* 0609:005 (2006)
76. Loeb A, Waxman E. *J. Cosmol. Astropart. Phys.* 5:3 (2006)
77. Waxman E, Bahcall J. *Phys. Rev. D* 59:023002 (1999)
78. Wang XY, Razzaque S, Meszaros P, Dai ZG. *Phys. Rev. D* 76:083009 (2007)
79. Budnik R, Katz B, MacFadyen A, Waxman E. *Astrophys. J.* 673:928 (2008)

80. Tamborra I, Ando S, Murase K. *J. Cosmol. Astropart. Phys.* 9:043 (2014)
81. Bartos I, Marka S. arXiv:1509.00983 [astro-ph] (2015)
82. Hopkins AM, Beacom JF. *Astrophys. J.* 651:142 (2006)
83. Lacki BC, Horiuchi S, Beacom JF. *Astrophys. J.* 786:40 (2014)
84. Gehrels N, Ramirez-Ruiz E, Fox DB. *Annu. Rev. Astron. Astrophys.* 47:567 (2009)
85. Mészáros P. *Astropart. Phys.* 43:134 (2013)
86. Mészáros P, Rees MJ. *Astrophys. J.* 530:292 (2000)
87. Rees MJ, Mészáros P. *Astrophys. J.* 628:847 (2005)
88. Beloborodov AM. *Mon. Not. R. Astron. Soc.* 407:1033 (2010)
89. Zhang B, Yan H. *Astrophys. J.* 726:90 (2011)
90. Murase K, Asano K, Terasawa T, Mészáros P. *Astrophys. J.* 746:164 (2012)
91. Waxman E, Bahcall JN. *Astrophys. J.* 541:707 (2000)
92. Murase K. *Phys. Rev. D* 78:101302 (2008)
93. Gao S, Asano K, Meszaros P. *J. Cosmol. Astropart. Phys.* 11:58 (2012)
94. Murase K, Kashiyama K, Mészáros P. *Phys. Rev. Lett.* 111:131102 (2013)
95. Bartos I, Beloborodov AM, Hurley K, Márka S. *Phys. Rev. Lett.* 110:241101 (2013)
96. Asano K, Meszaros P. *Astrophys. J.* 785:54 (2014)
97. Zhang B, Kumar P. *Phys. Rev. Lett.* 110:121101 (2013)
98. Aartsen MG, et al. *Astrophys. J. Lett.* 805:L5 (2015)
99. Ahlers M, Gonzalez-Garcia MC, Halzen F. *Astropart. Phys.* 35:87 (2011)
100. Abbasi R, et al. *Phys. Rev. Lett.* 106:141101 (2011)
101. Abbasi R, et al. *Nature* 484:351 (2012)
102. He HN, et al. *Astrophys. J.* 752:29 (2012)
103. Li Z. *Phys. Rev. D* 85:027301 (2012)
104. Hümmer S, Baerwald P, Winter W. *Phys. Rev. Lett.* 108:231101 (2012)
105. Kashiyama K, Murase K, Mészáros P. *Phys. Rev. Lett.* 111:131103 (2013)
106. Soderberg AM, et al. *Nature* 442:1014 (2006)
107. Campana S, et al. *Nature* 442:1008 (2006)
108. Howell EJ, Coward DM. *Mon. Not. R. Astron. Soc.* 428:167 (2013)
109. Murase K, Ioka K, Nagataki S, Nakamura T. *Astrophys. J. Lett.* 651:L5 (2006)
110. Liu RY, Wang XY, Dai ZG. *Mon. Not. R. Astron. Soc.* 418:1382 (2011)
111. Waxman E, Mészáros P, Campana S. *Astrophys. J.* 667:351 (2007)
112. Chevalier RA, Fransson C. *Astrophys. J. Lett.* 683:L135 (2008)
113. Mészáros P, Waxman E. *Phys. Rev. Lett.* 87:171102 (2001)
114. Aartsen MG, et al. *Astrophys. J.* 816:75 (2016)
115. Nakar E. *Astrophys. J.* 807:172 (2015)
116. Razzaque S, Mészáros P, Waxman E. *Phys. Rev. D* 68:083001 (2003)
117. Razzaque S, Meszaros P, Waxman E. *Phys. Rev. Lett.* 93:181101 (2004)
118. Ando S, Beacom JF. *Phys. Rev. Lett.* 95:061103 (2005)
119. Horiuchi S, Ando S. *Phys. Rev. D* 77:063007 (2008)
120. Horiuchi S, Ando S. *AIP Conf. Proc.* 1178:97 (2009)
121. Fraija N. *J. High Energy Astrophys.* 9:25 (2016)
122. Katz B, Sapir N, Waxman E. *Proc. IAU Symp.* 279:274 (2012)
123. Kashiyama K, et al. *Astrophys. J. Lett.* 769:L6 (2013)
124. Giacinti G, Bell AR. *Mon. Not. R. Astron. Soc.* 449:3693 (2015)
125. Gupta N, Zhang B. *Astropart. Phys.* 27:386 (2007)
126. Levinson A, Bromberg O. *Phys. Rev. Lett.* 100:131101 (2008)
127. Burrows DN, et al. *Nature* 476:421 (2011)
128. Metzger BD, Stone NC. *Mon. Not. R. Astron. Soc.* 461:948 (2016)
129. Dai L, Fang K. arXiv:1612.00011 [astro-ph] (2016)
130. Lunardini C, Winter W. arXiv:1612.03160 [astro-ph] (2016)
131. Beloborodov AM. *Mon. Not. R. Astron. Soc.* 438:169 (2014)
132. Smith MWE, et al. *Astropart. Phys.* 45:56 (2013)

133. Cowen DF, Keivani A, Tešić G. *Eur. Phys. J. Web Conf.* 116:10001 (2016)
134. Katz B, Waxman E, Thompson T, Loeb A. arXiv:1311.0287 [astro-ph] (2013)
135. Waxman E. arXiv:1511.00815 [astro-ph] (2015)
136. Adrián-Martínez S, et al. *J. Phys. G* 43:084001 (2016)
137. IceCube-Gen2 Collab., et al. arXiv:1510.05228 [astro-ph] (2015)
138. Shoemaker IM, Murase K. *Phys. Rev. D* 93:085004 (2016)
139. IceCube Collab., et al. arXiv:1612.05949 [astro-ph] (2016)
140. Aartsen MG, et al. *Eur. Phys. J. C* 76:531 (2016)
141. Vieregg AG. *Nucl. Phys. Proc. Suppl.* 229–232:545 (2012)
142. Barwick SW, et al. *Astropart. Phys.* 90:50 (2016)
143. Besson D, et al. *Proc. Sci.* ICRC2015:1105 (2016)
144. Ricci M. *J. Phys. Conf. Ser.* 718:052034 (2016)
145. Bigongiari C. arXiv:1606.08190 [astro-ph] (2016)
146. Giannios D. *Mon. Not. R. Astron. Soc.* 408:L46 (2010)
147. Dermer CD, Miller JA, Li H. *Astrophys. J.* 456:106 (1996)
148. Bykov AM, Mészáros P. *Astrophys. J. Lett.* 461:L37 (1996)
149. Petrosian V, Liu S. *Astrophys. J.* 610:550 (2004)
150. Brunetti G, Lazarian A. *Mon. Not. R. Astron. Soc.* 378:245 (2007)